Inorganic Chemistry

pubs.acs.org/IC

Article

Toward Reversible Crystalline-to-Amorphous Guest-Induced Transitions in Manganese(III) Carboxylate Metal−Organic Frameworks

Guillaume Esser, Robin Crits, Joséphine de Meester, Koen Robeyns, Tom Leyssens, Dmitry Chernyshov, Laura G. Graversen, Adam F. Sapnik, Kirsten M. Ø. Jensen, Catherine Dejoie, Meng He, Yaroslav Filinchuk,* Sophie Hermans,* and Timothy Steenhaut*

Cite This: https://doi.org/10.1021/acs.inorgchem.4c05337

Read Online

ACCESS | Metrics & More | Article Recommendations | Supporting Information

ABSTRACT: Metal−organic frameworks (MOFs) are an interesting class of inorganic/organic hybrid materials with a wide scope of applications. Although manganese is an abundant metal, the synthesis of Mn(III)-containing MOFs has not been widely studied due to the relative redox sensitivity of this species. We therefore investigated the self-oxidation of manganese(II) nitrate in the presence of aromatic dicarboxylic linkers in alcohols, discovering a series of new Mn(III)-MOFs. The obtained structures were analyzed through a combination of (synchrotron) X-ray diffraction and total scattering (pair distribution function analysis) experiments. In methanol, the syntheses led to new nonflexible members of the MIL-47/MIL-53 and MIL-69 families of MOFs, rare examples containing bridging methoxy anions. When using ethanol or 1-propanol, wine rack-like structures (named UcL-1 and UcL-2) with different Mn^{II}/Mn^{III} secondary building units are obtained. These demonstrate intriguing reversible crystalline-to-crystalline and crystalline-to-amorphous transitions upon guest exchange and release. The latter process involves strong correlated and noncorrelated structural distortions, paired with the creation of coordinatively unsaturated Mn^{III} sites. This work demonstrates that Mn(III)-containing carboxylate systems have the potential for the design of new functional MOF materials, including structures with tunable flexible behavior.

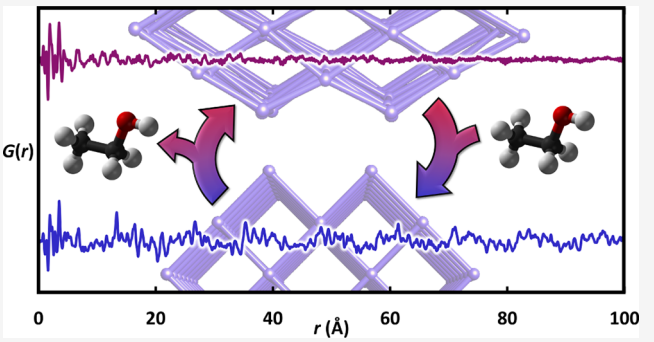

INTRODUCTION

Metal−organic frameworks (MOFs) are fascinating materials that find applications in many areas, including catalysis, guest sorption, drug delivery, gas storage, etc.[1−7] They are formed by the interconnection of metallic centers or clusters and organic linkers. The properties of those materials are due to an intricate combination between the building units (i.e., nature of metal and linker) and the resulting framework structure. To this day, thousands of different MOFs have been described throughout the literature. Those range from combinations of simple organic linkers and cheap and widely available metals to much more exquisite structures built from highly complex custom-made organic molecules and/or exotic metals, including actinides.[8,9]

With this ever-growing variety of synthetically obtainable MOFs, there is a particular class of frameworks that are less represented: the ones composed of metal centers with unstable low oxidation states. The reason behind this is that such frameworks, due to inherent redox considerations, often possess limited air stability, hence leading to more complicated manipulation and characterization. This is for example the case of Cr^{II} or Ti^{III}-containing MOFs.[10−13] Mn^{III} is another member of this category, with only few MOFs studied to date.[14−16] Some of the most representative examples among described Mn^{III}-MOFs are the highly complex MIL-100(Mn) and the more recently obtained MIL-101(Mn), as well as various frameworks containing Mn^{III} included in porphyrinic linkers.[17−20] In the latter case, however, manganese is often only included as part of the organic secondary building unit (SBU), while the inorganic SBU is composed of another metal species. Nevertheless, manganese is an abundant metal, and the scarce examples of Mn^{III}-MOFs have shown promising properties. Furthermore, and maybe unexpectedly, they have demonstrated quite good stability, mainly in combination with carboxylate linkers; MIL-100(Mn) for example has been

Received: December 14, 2024
Revised: February 12, 2025
Accepted: February 20, 2025

shown efficient in demanding catalytic applications, even in the presence of water or corrosive gases.[21−25]

With the aim of broadening the scope of existing of Mn^{III} MOFs, we here present the synthesis of various frameworks obtained from the solvothermal self-oxidation of manganese(II) nitrate in the presence of aromatic dicarboxylic acids in alcohols. We discovered that the nature of the alcohols directly influences the oxidation state and structural properties of the resulting frameworks, leading to the formation of distinct MOF architectures. Most interestingly, we obtained a new MOF with mixed III/II oxidation states which demonstrates a crystalline-to-disordered reversible structural expansion and contraction, as evidenced by means of (synchrotron) X-ray scattering experiments.

EXPERIMENTAL SECTION

Chemicals. Terephthalic acid (99+%), 2,6-naphthalenedicarboxylic acid (95%) and dimethyl sulfoxide (EMSURE ACS, for analysis) were purchased from Acros Organics. $Mn(NO_3)_2 \cdot 4H_2O$ (98%) was purchased from Sigma-Aldrich. $Mn(CH_3COO)_3 \cdot 2H_2O$ (97%) was purchased from Merck. *N*,*N*-dimethylformamide (DMF, HiPerSolv CHROMANORM), denatured ethanol (99%, Eurodenatured), methanol (technical), absolute ethanol (AnalaR NORMAPUR), dichloromethane (HiPerSolv CHROMANORM) and acetonitrile (HiPerSolv CHROMANORM) were purchased from VWR. 2,4-Pentanedione (99%) was purchased from Alfa Aesar.

Synthesis of MOFs. *MIL-53(Mn)-OMe.* A solution of manganese(II) nitrate tetrahydrate (0.314 g, 1.25 mmol) in 2 mL of methanol was added to a suspension of terephthalic acid (0.296 g, 1.78 mmol) in 8 mL of methanol. The mixture was then transferred to a 25 mL screw-capped bottle, and a magnetic stirring bar was added. The bottle was then closed and maintained in an oil bath using a clamp fixed to the cap. The solution was stirred at 120 °C for 3 h and then washed by centrifugation (8000 rpm for 1 min) with hot DMF and then with methanol. Finally, the powder was dried under vacuum at 45 °C for several hours (Yield: 0.0531 g, 17%). *Note:* The same procedure can be applied by substituting Mn(II) nitrate for Mn(III) acetate dihydrate (0.223 g, 0.96 mmol). (Yield: 0.1397 g, 58%).

MIL-69(Mn)-OMe. A solution of manganese(II) nitrate tetrahydrate (2.510 g, 10 mmol) in 4 mL of methanol was added to a suspension of 2,6-naphthalenedicarboxylic acid (2.162 g, 10 mmol) in 36 mL of methanol. The mixture was then transferred to a 200 mL Teflon-lined autoclave and heated for 3 h at 120 °C. The obtained dark brown solid was then filtered on a nylon membrane and washed at least three times with hot DMF. A second washing was then performed with methanol. Finally, the powder was dried under vacuum at 45 °C for several hours.

UcL-1 (Université catholique de Louvain-1/Small Scale Synthesis). A solution of manganese(II) nitrate tetrahydrate (2.510 g, 10 mmol) in 4 mL denatured ethanol was added to a suspension of terephthalic acid (2.366 g, 14.2 mmol) in 36 mL of the same solvent. The mixture was then transferred to a 200 mL Teflon-lined autoclave and heated for 4 h at 125 °C in an oven. The obtained dark brown solid was filtered on a nylon membrane and washed at least three times with hot DMF. A second washing was then performed with denatured ethanol. Finally, the powder was dried under vacuum at 45 °C for several hours. (Yield: 0.7825 g, 12%). *Note:* the sample from the small scale synthesis was used for laboratory powder X-ray diffraction (PXRD) experiments.

Optimized Scale-up Procedure for the Synthesis of UcL-1. Manganese(II) nitrate tetrahydrate (15.061 g, 60 mmol), terephthalic acid (6.645 g, 40 mmol), and 130 mL of denatured ethanol were added to a 250 mL glass screw-capped bottle. The mixture was then heated in an oven for 4 h at 120 °C. The obtained dark brown solid was filtered on a nylon membrane and washed at least three times with hot DMF. A second washing was then performed with denatured ethanol. Finally, the powder was dried under vacuum at room temperature overnight. (Yield: 3.8584 g, 36%). *Note* 1: substitution of Mn(II) nitrate by Mn(III) actetate dihydrate resulted in a clear solution with unreacted terephthalic acid after heating. *Note* 2: the scaled-up sample was used for synchrotron experiments.

Single Crystals. Singe crystals were recovered from the suspension after reaction. Some very small brown crystals of UcL-1 (40 μm × 5 μm × 5 μm) were carefully selected from the suspension composed mainly of unreacted (recrystallized) H_2BDC (large white crystals) and used for structure solution by synchrotron X-ray diffraction at the Swiss-Norwegian Beamlines (SNBL) at the European Synchrotron Radiation Facility (ESRF). Many attempts were necessary before being able to pick up a well diffracting crystal, illustrating the high sensitivity toward desolvation, leading to disordered phases and damage to the single crystal.

UcL-2. The synthesis with 1-propanol was performed in the same way as described for UcL-1, by replacing ethanol by 1-propanol both as synthesis and washing solvent and lowering the reaction time to 45 min. The outcome of the synthesis with 1-propanol seems however much more sensitive to temperature and reaction time, small changes to the procedure leading to other, unidentified, crystalline phases.

Solvent Exchange and Reversibility Tests. Reversible solvent exchange tests on UcL-1 were performed on approximately 50 mg of as-synthesized sample which was transferred to a 4 mL screw-capped vial with 3 mL of the solvent for exchange. The samples were allowed to soak for approximately 30 min and subsequently collected by membrane filtration (nylon membrane, 0.22 μm pore size) and quickly dried under a stream of compressed air before subjecting part of the sample to PXRD analysis in a capillary. Reversibility of the exchange was performed by immersing the remaining powder in approximately 3 mL of ethanol in a 4 mL screw-capped vial for 1 h. The sample was then recovered by membrane filtration and analyzed by PXRD in a capillary.

Instruments and Methods. *Lab PXRD* analyses were performed using a MAR345 diffractometer with X-rays generated by an Incoatec Microfocus Source^{HIGHBRILLIANCE} (IμS^{HIGHBRILLIANCE}) Mo ELM47 operating at 50 kV and 1000 μA (λ = 0.71073 Å). Samples were loaded in 0.7 mm glass capillaries (Hilgenberg GmbH). Diffraction data were integrated using the Fit2D software (a 0.3 mm diameter capillary filled with LaB_6 was used as calibrant). *Synchrotron X-ray powder and single crystal diffraction* experiments were performed on the multipurpose PILATUS@SNBL diffractometer at BM01 at the Swiss-Norwegian beamlines (SNBL) at the European Synchrotron Radiation Facility (ESRF) in Grenoble (France). For powder diffraction, the samples were loaded into 0.5 mm diameter glass capillaries (Hilgenberg GmbH) and rotated during exposure to the X-ray beam. Heating of the sample was performed with a custom-made furnace in ramping

https://doi.org/10.1021/acs.inorgchem.4c05337
Inorg. Chem. XXXX, XXX, XXX−XXX

mode during the measurement (10 °C/min). Data were recorded using a PILATUS2M detector and preprocessed and treated with the SNBL ToolBOX and BUBBLE softwares, respectively.[26] Structure solution and refinements were performed using the FOX software and Fullprof suite.[27,28] Single crystals were flash cooled to 150 K in a gaseous N_2 stream using an Oxford Cryostream system prior to the measurement. A phi scan with 1° increments was measured for a total of 360 images. Data integration and reduction were carried out using the CrysAlis^{PRO} software package, and the implemented absorption correction was applied.[29] The structures were solved by dual space direct methods (SHELXT) and refined against F^2 by SHELXL-2019/3.[30,31] All non-hydrogen bonds were refined anisotropically, hydrogen atoms were added in calculated positions and refined in riding mode, with temperature factors 1.2 times higher than their parent atoms (1.5 for methyl hydrogens). Void cavities were treated by the Squeeze algorithm as implemented in PLATON to take into account the contribution of the diffuse electron density.[32] *Synchrotron total scattering experiments* were performed on the ID22 beamline at ESRF, using a flat panel PerkinElmer XRD 1611CP3 detector and an X-ray energy of 60 keV (λ = 0.20665 Å), allowing to use the instrument in rapid-acquisition pair distribution function (RA-PDF) mode.[33,34] The samples were loaded into a 0.7 mm glass capillary (Hilgenberg GmbH) and spun during the whole experiment. A custom in-house heat blower was used to control the temperature of the samples, which were measured in isothermal mode (exposure time of 20 min per pattern). The scattering pattern from an empty capillary was also measured, which subsequently was subtracted as a background to obtain the pattern from the sample. Data were integrated using pyFAI and the PDFs were obtained from the scattering patterns through data reduction using the xPDFsuite software with a Q_{min} and a Q_{max} of 0.4 and 19.0 Å^{-1}, respectively, and r_{poly} of 0.9 Å.[35] Simulation of PDFs for comparison were obtained through the Debye Calculator software, using discrete models cut out from the MOF crystal structure using the Vesta software.[36,37] Thermogravimetric analysis/differential thermal analysis (*TGA/DTA*) measurements were recorded on a Mettler Toledo TGA/DSC 3+ STARe system equipped with a TGA/DTA sample holder. Analyses were performed in Al_2O_2 crucibles under an oxygen or nitrogen flow of 100 mL/min and a heating rate of 10 °C/min from 25 to 850 °C.

RESULTS AND DISCUSSION

Synthesis of MIL-53(Mn) in Methanol. We first attempted the fabrication of Mn(III)-MOFs in methanol by self-oxidation of manganese(II) nitrate, inspired by the synthesis of MIL-100(Mn), previously described by Reinsh and Stock.[17] In this procedure, it was shown that the nitrate ions of this specific salt enable the *in situ* oxidation of the Mn^{2+} cations into Mn^{3+} in specific solvents. When the reaction was performed with terephthalic acid (benzene-1,4-dicarboxylic acid, H_2BDC), brown MOF particles were obtained, which were analyzed by powder X-ray diffraction (PXRD, see Figure S1). Although the formation of a framework composed of Mn_3-μ_3-oxo clusters, such as the ones of MIL-100(Mn), could be expected, the pattern did not reveal any resemblance with known topologies of terephthalate MOFs containing similar trinuclear metal-oxo clusters (e.g., MIL-101 or MIL-88B derivatives).[38,39] Some small crystals of sufficient size could be isolated to solve the structure from single crystal synchrotron X-ray diffraction, revealing that the compound is instead a topological analogue of the well-known MIL-53 type framework (Figures 1A,B, S2 and Table S1), and has the

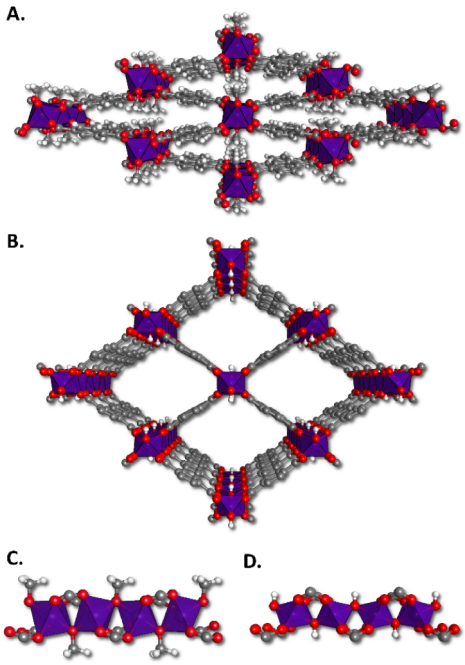

Figure 1. Crystal structures of (A) MIL-53(Mn)-OMe and (B) MIL-53(Al) in its open-pore form (hydrogen of BDC^{2-} omitted for clarity) with detail of the inorganic SBUs displaying the (C) μ_2-OMe and (D) μ_2−OH bridges in the respective MOFs.

chemical formula $Mn^{III}(OCH_3)(C_8H_4O_4)$. In this MOF, Mn has a + III oxidation state, as confirmed by analysis of bond lengths and charge balance (Table S2).

It should be noted that the MOF was however obtained in a rather low yield when using manganese(II) nitrate as precursor (17%). This could be improved by using manganese(III) acetate instead (58% yield). In each case, the MOF was obtained in a resulting clear solution, indicating that no solubilized Mn^{3+} remained after reaction. From this, it can be deduced that reduction of solubilized Mn^{3+} by methanol is in competition with the formation of the MOF, which stabilizes Mn^{III} in the solid form. The reducing nature of the reaction medium is also likely the reason why Mn^{IV} is not present in the final MOF, although the latter is a more stable oxidation state for Mn. Additionally, we noted that adding water to the reaction mixture did not lead to the formation of any MOF. This suggests that the presence of water interferes with the formation of the desired phase, possibly hindering the oxidation process of Mn from the +II to +III state, and thus preventing crystallization of the MOF.

Structure and Nonflexibility of MIL-53(Mn)-OMe. MIL-53 has previously been reported with various trivalent metals such as Cr, Al, Fe, Sc and Ga, as well as with V. In the latter case, however, the framework is termed MIL-47, due to historical reasons as a structural similarity between the V and Cr analogues was first unnoticed. The MIL-53/MIL-47 series of MOFs are all built from chain-like inorganic secondary building units (SBUs), in which the metal centers are interconnected by the carboxylate units of the clusters, and by monovalent μ_2 bridging anions (Figure 1B). Those bridging

https://doi.org/10.1021/acs.inorgchem.4c05337
Inorg. Chem. XXXX, XXX, XXX−XXX

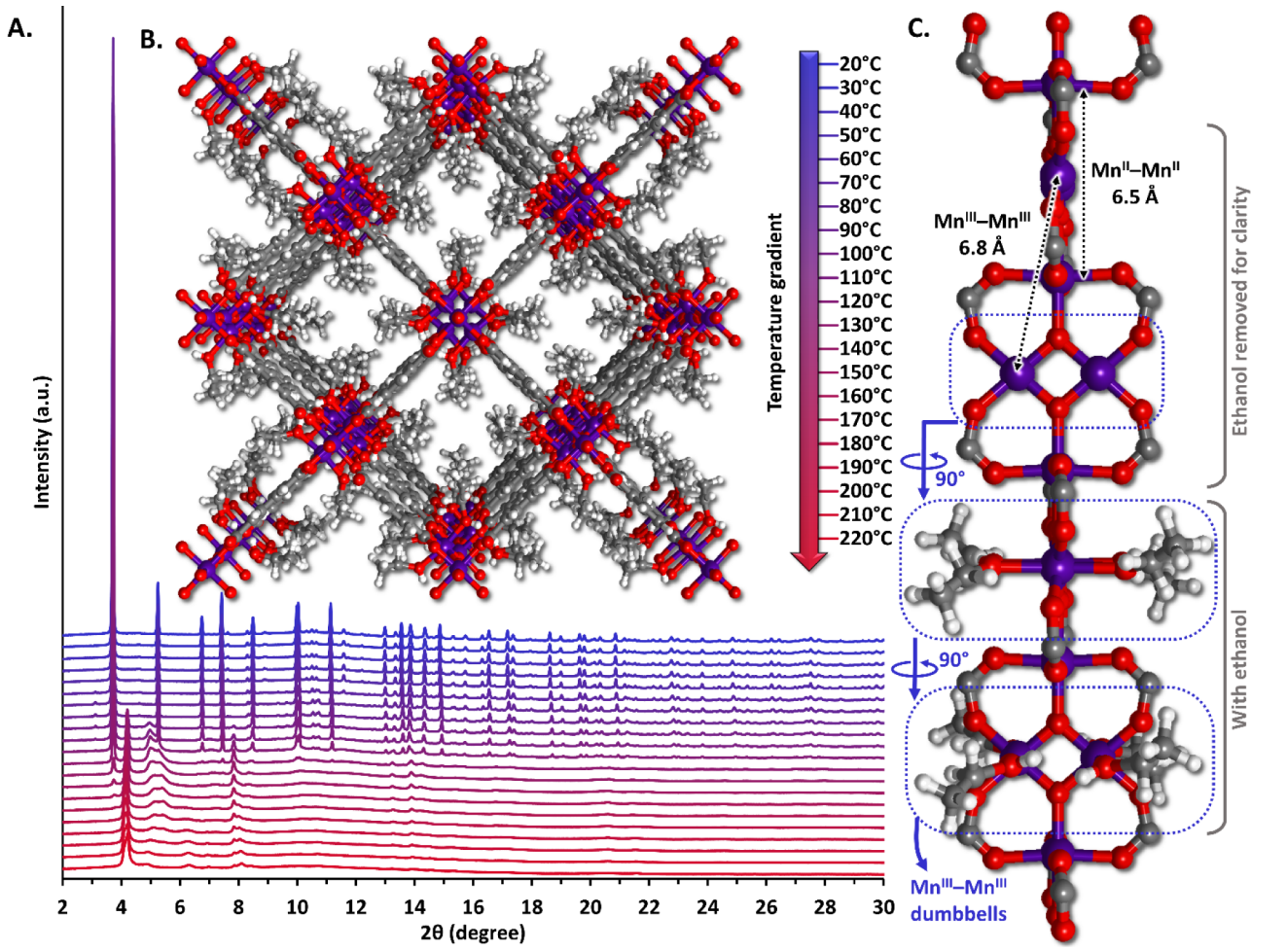

Figure 2. (A) Synchrotron variable temperature X-ray diffraction data of UcL-1 (λ = 0.75334 Å) with (B) representation of the structure viewed along the *c* axis and (C) detail of the chain SBU, with the Mn−Mn dumbbells highlighted, together with their four surrounding ethanol ligands (two per Mn). The disorder, visible in the crystallographic information file in the Supporting Information, has been omitted for clarity.

anions are classically μ_2-hydroxyls, or, although less frequently encountered, μ_2-fluorides (Figure 1D).[40]

Interestingly, our Mn analogue, which is further called "MIL-53(Mn)-OMe", possesses μ_2-methoxy bridging anions instead of the classical OH^- or F^- anions (Figure 1C), which originate from the use of methanol as synthesis solvent. The presence of the μ_2-OMe moieties was confirmed by thermogravimetric analysis (TGA, see Figure S3). Recently, it has been shown that, in the case of an interpenetrated MIL-53(Sc) derivative (termed "GUF-1"), μ_2-OH bridging anions could be replaced by μ_2-OMe in the presence of methanol under the extreme conditions provided by a diamond anvil cell.[41] In our case, however, the introduction of the bridging μ_2-OMe is performed through direct synthesis under much milder conditions. The potential replacement of −OMe groups by OH moieties was investigated by immersing the material in water at room temperature for 1 week. However, this treatment resulted in a weakly diffracting powder, indicating framework degradation (see Figure S4).

In previously reported MIL-53/MIL-47 frameworks, the interconnection of the metal SBUs with the organic linkers forms a wine-rack like structure, which in some cases leads to flexibility, depending on the nature of the metals composing the framework and the eventual presence of supplementary organic functional groups on the linkers.[40,42] We investigated several stimuli to evaluate the potential flexibility of the MIL-53(Mn)-OMe MOF, including heat, immersion in various solvents and exposure to CO_2 gas. Unfortunately, a combination of *ex situ* and *in situ* PXRD analyses showed that none of the tested stimuli were able to lead to any observable structural transition between open- and closed-pores states (i.e., breathing) in this MOF (Figures S5−S7).

Synthesis and Nonflexibility of MIL-69(Mn)-OMe. An extended linker strategy, using 2,6-naphthalenedicarboxylic acid (H_2NDC) instead of H_2BDC, was attempted to evaluate the impact of the linker length on the properties of the modified MOF. Synchrotron powder X-ray diffraction (Figure S8) shows that the isolated brown powder, identified as MIL-69(Mn)-OMe, possesses a topology similar to MIL-69, which is an extended version of the MIL-53 MOF, which has previously been reported with trivalent metal centers, including Al, V and Ga.[43−45] TGA however indicates that, similarly to MIL-53(Mn)-OMe, the classically encountered μ_2−OH bridging ligands are replaced by μ_2-OMe moieties (Figure S9). Although MIL-69 has also been reported to have a possible breathing mechanism, MIL-69(Mn)-OMe did not show such behavior under thermal stimulus (Figures S10).[46] Other stimuli were not explored for this MOF, given the reported more difficult breathing of MIL-69 compared to MIL-

https://doi.org/10.1021/acs.inorgchem.4c05337
Inorg. Chem. XXXX, XXX, XXX−XXX

53 MOFs, attributed to increased π-stacking of the NDC^{2-} linkers compared to BDC^{2-}.

Synthesis in Ethanol and Structure of UcL-1. As syntheses in methanol yielded MOFs with μ_2-OMe, we investigated the possibility of incorporating larger bridging anions, such as ethoxy or propoxy moieties, to force the opening of porous channels. A first synthesis was thus performed with H_2BDC in ethanol as solvent, with the aim to incorporate the μ_2-OEt anion. The obtained brown powder, which was termed UcL-1 ("Université catholique de Louvain-1"), was highly crystalline upon washing with DMF and subsequent treatment with ethanol (Figure 2). The structure of the ethanol-solvated MOF could be solved through synchrotron X-ray diffraction on a small single crystal (see SI for details and Table S3), revealing a tetragonal unit cell and the chemical formula $Mn^{II}Mn_2^{III}O_2(C_8H_4O_4)_2(C_2H_5OH)_4$. Surprisingly, the inorganic SBU of UcL-1 is very different from those of MIL-53(Mn)-OMe and MIL-69(Mn)-OMe. In this case, chain-like SBUs composed of alternating single Mn^{II} atoms and Mn^{III}−Mn^{III} dumbbells are obtained, which are interconnected by μ_3-O bridging anions and the (μ_2) carboxylate functions of the linkers (Figure 2C and Mn−O distances in Table S2). The Mn−Mn dumbbells repeat alternately, with a 90° rotation around the *c*-axis. The octahedral coordination sphere of each of the Mn atoms in the dumbbells is completed by two ethanol molecules, acting as ligands, instead of the expected ethoxy functions. Although there are some reports describing tetrameric units with M^{III}−M^{III} dumbbells (M = Fe^{III}, Mn^{III} and Cu^{II}) in MOFs or molecular complexes,[47−49] those are generally isolated SBUs, with a single oxidation state for all metal centers. UcL-1 thus has a unique type of chain-like SBU formed by interconnected tetrameric subunits containing metals in two distinct oxidation states. In addition, this structure could only be obtained when using manganese(II) nitrate as precursor for the synthesis, as substitution by manganese(III) acetate in this case did not lead to the formation of any MOF.

Guest-Induced Transformations in UcL-1. Interestingly, the linkers interconnect the SBUs in a wine-rack like structure, presenting large open channels, which have potential for guest exchange. The possibility to perform solvent exchange in UcL-1 was evaluated by synchrotron PXRD experiments on samples obtained after immersion in dimethyl sulfoxide, dimethylformamide, dichloromethane, acetonitrile, and acetone (Figure S11). Those evidenced large changes in the diffraction patterns, such as crystalline-to-crystalline phase transitions, indicating successful solvent exchange and breathing behavior. Heating up the solvent-exchanged samples led to a series of structural transitions, mostly of crystalline-to-crystalline nature, although some crystalline-to-disordered changes were observed as well (Figure S12). The structures of those guest-exchanged UcL-1 samples were not solved, owing to the difficulty in achieving satisfactory Rietveld refinements for disordered solvent molecules located in the channels. The reversibility of the process was however demonstrated by lab PXRD experiments consisting of re-exposure of the solvent-exchanged samples to ethanol. This led to complete or partial (for DMSO and DMF, which are typically more difficult to exchange) recovery of the initial structure (Figure S13).

The possibility to activate the MOF (i.e., removing guest molecules) by heating was investigated through thermogravimetric analysis and *in situ* X-ray scattering experiments. TGA indicates that the sample loses up to 6.3 wt % between room temperature and 135 °C (Figure S14), which corresponds to the removal of one out of four ethanol molecules from the as-synthesized MOF ($Mn^{II}Mn^{III}_2O_2(BDC)_2(EtOH)_4$). *In situ* synchrotron PXRD shows that when heated from room temperature to 120 °C, relative intensities of the diffraction peaks gradually change, in accordance with guest release (Figure 2). This is particularly visible for the first two diffraction peaks at 3.7 and 5.25 degrees (Figure 3). In this

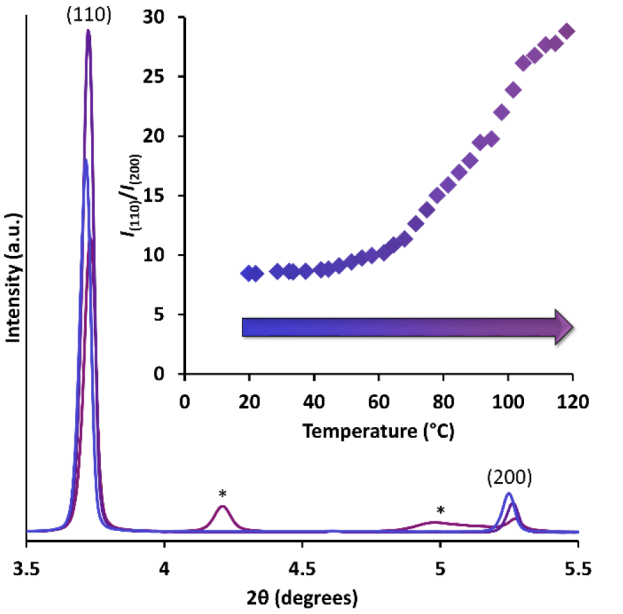

Figure 3. Zoomed-in PXRD patterns of UcL-1 at selected temperatures (20, 80, and 120 °C), with the ratio of the integrated areas of the (110) and (200) peaks versus temperature shown in the inset. The disordered phase starts to appear at approximately 95 °C, with its features marked by asterisks.

temperature range, only negligible Bragg peak shifts are observed, indicating that the open pore structure is maintained while the first ethanol molecules leave the framework. The appearance of a minor diffraction peak at 3.12° around 70 °C, along with the disappearance of the (213) reflection at 11.59° (see Figure S15), indicates the possible formation of a superstructure paired with a change in symmetry. This is linked to the removal of half an ethanol molecule per Mn−Mn dumbbell, on average, as suggested by the weight loss observed on the TGA. This is furthermore accompanied by a change in the evolution of the relative intensities ratio of the (110) and (200) peaks with temperature (Figure 3, inset). A LeBail refinement and identification of the associated reflections further support a superlattice with a doubled *c* parameter (Figure S16).

Above 120 °C, the further removal of Mn-coordinated ethanol molecules leads to a loss of crystallinity paired with a significant structural change (see Figure 2). In particular, the initially very intense Bragg peak at 3.71° from the fully solvated MOF disappears and a new peak appears at 4.15°, indicating a pore closure phenomenon (Figure S17A). Both phases coexist between 95 and 150 °C, with a linear rate of disappearance and appearance of both phases until 120 °C, after which a nonlinear rate is observed (Figure S18). This coincides with a sudden weight loss on the TGA curve between 120 and 150 °C, suggesting that the phase change and pore closure is synergistic with the release of the second ethanol molecule

https://doi.org/10.1021/acs.inorgchem.4c05337
Inorg. Chem. XXXX, XXX, XXX−XXX

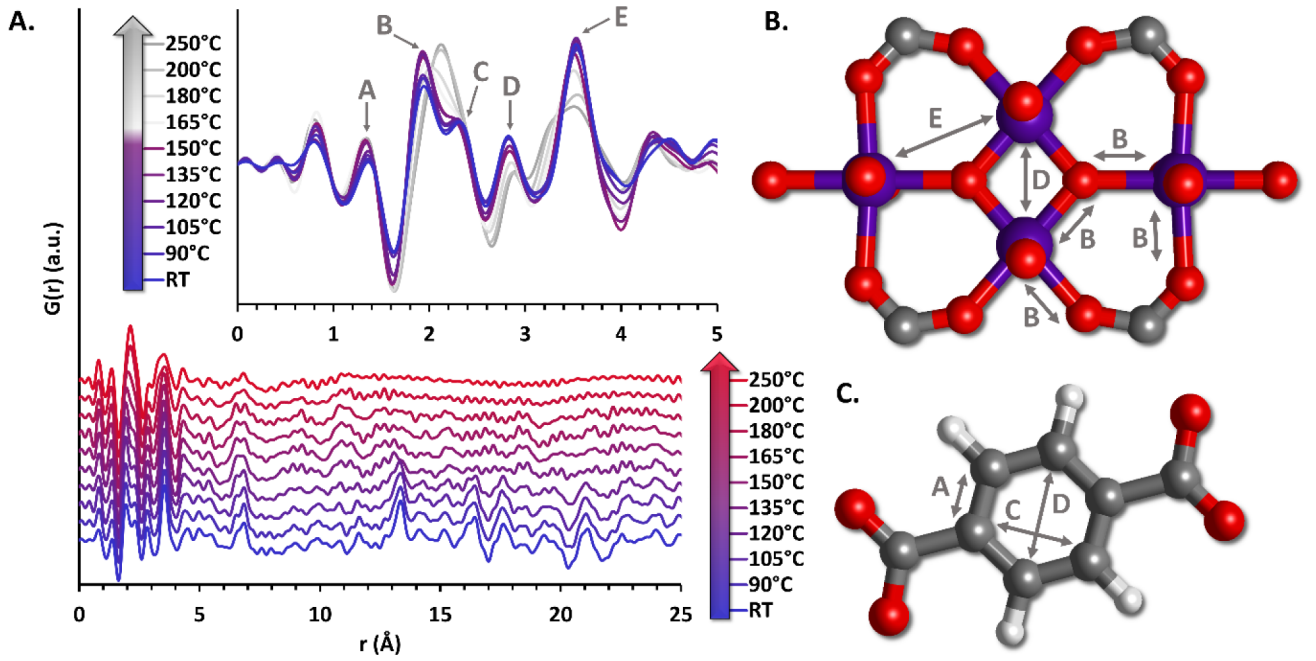

Figure 4. (A) Evolution of the pair distribution function of the UcL-1 MOF during thermal activation and attribution of the short-range pairs (inset) in the (B) inorganic SBU and (C) terephthalate linker.

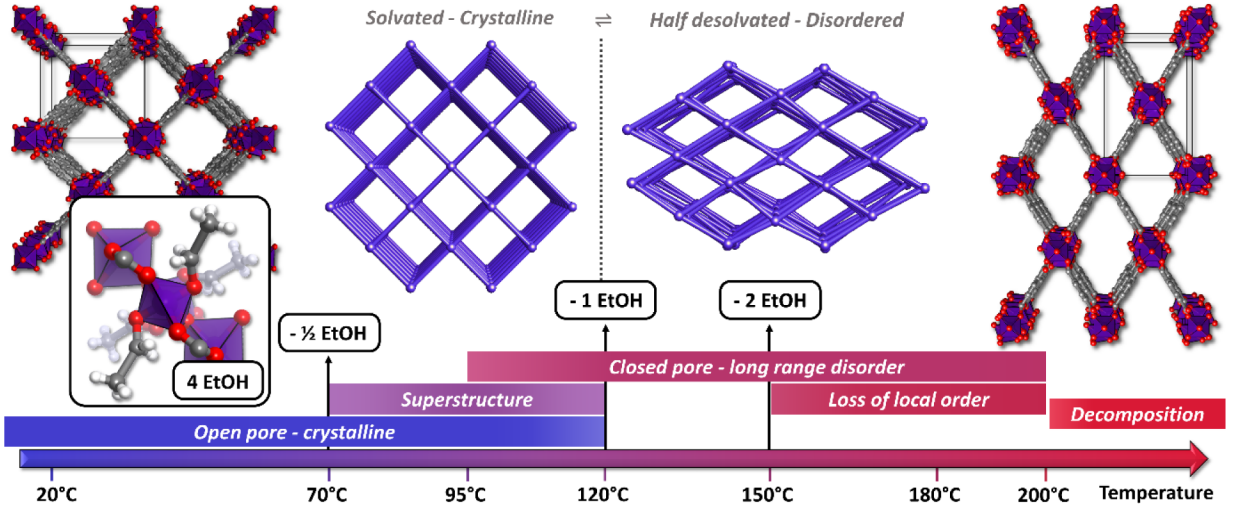

Figure 5. Summary of structural changes induced in the UcL-1 MOF by thermal ethanol removal. Idealized crystal structures on the extreme left and right represent the strong correlated (unit cell) deformation, whereas the middle part illustrates the combination of strong correlated and uncorrelated (disorder) distortions in the MOF. Ethanol molecules and hydrogens are omitted from those structures for clarity. The inset on the left represents part of the SBU with the Mn^{III}–Mn^{III} dumbbell initially coordinated to four ethanol molecules, along with the two neighboring Mn^{II} atoms. The structural changes are correlated with the average number of ethanol molecules removed from this structural subunit, as determined from TGA.

from the Mn–Mn dumbbell (Figure S14). It is worth mentioning that, since all ethanol molecules are equivalent, it is impossible to determine which one is released first. The total weight loss before decomposition, corresponding to the temperature at which notable differences are observed between TGA curves under O_2 and N_2 atmospheres (~200 °C), coincides with the removal of about half of the ethanol molecules. These observations suggest that thermal activation can create approximately one coordinatively unsaturated site (CUS) on each metal center of the Mn^{III}–Mn^{III} dumbbells. The first CUS is created without structural deformation, whereas the formation of the second CUS is paired with pore closure and strong increase of disorder. The positions of the main Bragg peaks, together with geometrical constraints of the framework, enabled us to determine that during this process the unit cell of the MOF was mainly elongated along the *a* axis from 16.4 to 19.6 Å, and contracted along the *b* axis to 12.2 Å (see details about the determination of the unit cell axes in Figure S17).

As the PXRD patterns at temperatures above 120 °C indicate a strong increase in disorder, the activation process was further characterized through an *in situ* total scattering experiment. This enabled us to extract the temperature-dependent pair distribution functions (PDF, Figure 4A), which contain structural information included in both the Bragg peaks and the diffuse scattering.[50,51] Sharp peaks from the local

https://doi.org/10.1021/acs.inorgchem.4c05337
Inorg. Chem. XXXX, XXX, XXX–XXX

structure were observed up to 4 Å, and could be assigned to Mn−O (1.9 and 2.3 Å), C−C (1.4, 2.3, and 2.8 Å), and Mn^{II}−Mn^{III} (2.8 and 3.5 Å) distances from the SBU and linker by correlation with distances extracted from the crystal structure (see Figures 5, S19 and Table S4 and simulations in Figure S20). At room temperature, peaks were observed up to 100 Å and peaks still extend up to 85 Å at 120 °C, (Figures S21A), indicating long-range order, in accordance with the highly crystalline nature observed by PXRD. Upon heating above 120 °C, peaks in the PDF disappear above 35 Å. The short-range order below 4 Å is however maintained up to 150 °C (see inset of Figure 4A), indicating that the metal-to-linker bonds remain intact up to this temperature. This evidence that neither the SBUs nor the aromatic linker are degraded during the heating process.

Closer inspection of the PDF reveals changes in the peaks between 6.5 and 6.8 Å, typical of the distances between two Mn^{II} sites or two Mn^{III} dumbbells (see Figure 2C), when reaching 120 °C. This might indicate that the linearity of the inorganic SBUs is partially lost at this temperature, with the chains likely distorted upon guest removal. The long-range order at >7 Å is even more affected by the thermal treatment between 120 and 180 °C, with much weaker signal intensities. New signals are however observed at 11 and 18 Å between 135 and 180 °C, in accordance with a structural change, as observed from PXRD. Furthermore, a long-range density modulation pattern at high r (see Figure S21B) can be observed in the PDFs, between room temperature and 180 °C, typical for porous materials with periodically spaced voids such as MOFs.[52] Those patterns, which change during the structural distortion at 120 °C, could be successfully approximated by a pseudoatomic model using the unit cells determined from PXRD, showing good agreement of the long-range density modulation of the PDF and the structural models before and after pore closure (Figure S21B). From 180 °C onward, the short-range order (below 4 Å, see inset in Figure 4A) is strongly affected by the process, indicating possible degradation of the SBUs, with complete loss of those atom pair distances above 200 °C, evidencing framework decomposition. This is further supported by simulations of the short-range PDF (Figures S22 and S23) and by the differences in the thermograms recorded under O_2 and N_2 atmospheres above 200 °C, indicating an oxidative process involving atmospheric oxygen (Figure S14). Importantly, the reversibility of the ethanol removal was further probed by re-exposing a disordered sample (treated at 150 °C) to ethanol at room temperature. PXRD analysis showed that upon this exposure, the initial crystal structure was successfully recovered (Figure S24)

We would like to emphasize that reversible order-to-disorder transitions in MOFs have only recently started to be addressed, mainly in MOF-5 derivatives modified with alkoxy chains on their linkers.[53,54] Such transition to disordered states has been termed "frustrated flexibility" and explained by incompatibility of intraframework dispersion forces with geometrical constraints of the SBUs. In the case of the reported MOF-5 derivatives, however, no coordinatively unsaturated sites were involved, and the observed distortion of unit cell remained minimal. To the best of our knowledge, the case of UcL-1 is thus unprecedented in the fact that a combination of both strongly correlated anisotropic (change of crystal system) and uncorrelated (random disorder) distortions occur, with the loss of coordinated guest molecules, as illustrated in Figure 5.

Synthesis of UcL-2 in 1-Propanol. By changing the synthesis solvent from ethanol to 1-propanol, a brown highly crystalline powder could be obtained, although the synthesis turned out to be more sensitive to the reaction temperature and time (Figure S25). Close inspection of the X-ray diffraction pattern of this sample, which was named UcL-2, revealed that the diffraction peaks are located at identical positions as for UcL-1, with however differences in relative peak intensities. The structure of the MOF obtained in 1-propanol is thus very similar to the one of UcL-1, with a probable composition of $Mn^{II}Mn_2^{III}O_2(C_8H_4O_4)_2(C_3H_7OH)_4$, with likely coordinated 1-propanol instead of ethanol. The guest exchange behavior in this MOF was not investigated, but is expected to be similar to the one of UcL-1.

CONCLUSIONS

We demonstrated that the use of manganese(II) nitrate in conjunction with aromatic dicarboxylic (terephthalic or 2,6-naphthalenedicarboxylic) acids in various alcohols leads to the formation of a series of Mn(III) containing MOFs. Synthetic control over the SBUs could be achieved through selection of the alcohol solvent used for the synthesis. When the synthesis was performed in methanol, new members of the MIL-53/MIL-47 and MIL-69 families were obtained with BDC^{2-} and NDC^{2-} linkers, respectively. However, by contrast to the previously reported MOFs of these topologies, the obtained MIL-53(Mn)-OMe and MIL-69(Mn)-OMe MOFs possess μ_2-OMe bridging anions instead of the μ_2−OH or μ_2-F moieties that are usually incorporated through direct synthesis. Those two MOFs however did not present any breathing behavior as previously observed for their analogues based on other metals and bridging anions. Most interestingly, when the synthesis was performed in longer chain alcohols, a completely different structure was obtained. The UcL-1 and UcL-2 MOFs, obtained from terephthalic acid in respectively ethanol and 1-propanol, displayed a highly crystalline open pore structure. Furthermore, the chain-like SBUs of those MOFs, composed of alternating Mn^{II} sites and Mn^{III}−Mn^{III} dumbbells are, to the best of our knowledge, unprecedented in MOFs. UcL-1 in particular presents potential in guest sorption through changes between ordered and disordered states, probed through a combination of X-ray diffraction and scattering experiments. Solvent exchanges led to crystalline-to-crystalline phase transitions, depending on the nature of the guest molecule. Thermal removal of ethanol from UcL-1 leads to a disordered structure with coordinatively unsaturated Mn^{III} sites, through a combination of reversible strong correlated and noncorrelated framework distortions, with preservation of local order. This transition is reversible upon exposure to ethanol. In summary, these findings pave the way to the design of new functional Mn^{III}-containing MOFs with intricate guest sorption behavior.

ASSOCIATED CONTENT

Supporting Information

The Supporting Information is available free of charge at https://pubs.acs.org/doi/10.1021/acs.inorgchem.4c05337.

PXRD patterns, Rietveld and LeBail refinements, crystallographic tables, TGA, pair distribution functions, modeling (PDF). The raw datasets collected at ESRF are available at https://doi.esrf.fr/10.15151/ESRF-DC-2039871980.

https://doi.org/10.1021/acs.inorgchem.4c05337
Inorg. Chem. XXXX, XXX, XXX−XXX

Accession Codes

Deposition Numbers 2403129−2403130 contain the supplementary crystallographic data for this paper. These data can be obtained free of charge via the joint Cambridge Crystallographic Data Centre (CCDC) and Fachinformationszentrum Karlsruhe Access Structures service.

AUTHOR INFORMATION

Corresponding Authors

Yaroslav Filinchuk − *Institut IMCN, Université catholique de Louvain, Louvain-la-Neuve 1348, Belgium;* orcid.org/0000-0002-6146-3696; Email: yaroslav.filinchuk@uclouvain.be

Sophie Hermans − *Institut IMCN, Université catholique de Louvain, Louvain-la-Neuve 1348, Belgium;* orcid.org/0000-0003-4715-7964; Email: sophie.hermans@uclouvain.be

Timothy Steenhaut − *Institut IMCN, Université catholique de Louvain, Louvain-la-Neuve 1348, Belgium;* orcid.org/0000-0003-2881-9440; Email: timothy.steenhaut@uclouvain.be

Authors

Guillaume Esser − *Institut IMCN, Université catholique de Louvain, Louvain-la-Neuve 1348, Belgium*

Robin Crits − *Institut IMCN, Université catholique de Louvain, Louvain-la-Neuve 1348, Belgium*

Joséphine de Meester − *Institut IMCN, Université catholique de Louvain, Louvain-la-Neuve 1348, Belgium*

Koen Robeyns − *Institut IMCN, Université catholique de Louvain, Louvain-la-Neuve 1348, Belgium;* orcid.org/0000-0002-4763-4217

Tom Leyssens − *Institut IMCN, Université catholique de Louvain, Louvain-la-Neuve 1348, Belgium;* orcid.org/0000-0001-7916-1373

Dmitry Chernyshov − *European Synchrotron Radiation Facility (ESRF), Grenoble 38000, France;* orcid.org/0000-0001-7738-9358

Laura G. Graversen − *Department of Chemistry, University of Copenhagen, Copenhagen 2100, Denmark*

Adam F. Sapnik − *Department of Chemistry, University of Copenhagen, Copenhagen 2100, Denmark;* orcid.org/0000-0001-6200-4208

Kirsten M. Ø. Jensen − *Department of Chemistry, University of Copenhagen, Copenhagen 2100, Denmark;* orcid.org/0000-0003-0291-217X

Catherine Dejoie − *European Synchrotron Radiation Facility (ESRF), Grenoble 38000, France;* orcid.org/0000-0003-3313-3515

Meng He − *European Synchrotron Radiation Facility (ESRF), Grenoble 38000, France*

Complete contact information is available at: https://pubs.acs.org/10.1021/acs.inorgchem.4c05337

Notes

The authors declare no competing financial interest.

ACKNOWLEDGMENTS

The authors gratefully acknowledge the financial support provided by the Fonds de transition énergétique (H2Be project), the support from the FNRS through CdR grants (CdR J.0073.20 and CdR J.0078.24), PDR grant (T.0262.20), and the Win4Excellence program (grant 2310142). KMØJ, LGG, and AFS would like to thank the Villum Foundation (42079) and the Danish National Research Foundation (DNRF149) for funding. The European Synchrotron Radiation Facility (ESRF) is acknowledged for granting access to their facilities under proposal numbers CH-6536, CH-6690, and CH-6877 and for the invaluable resources provided.

REFERENCES

(1) Yang, D.; Gates, B. C. Characterization Structure, and Reactivity of Hydroxyl Groups on Metal-Oxide Cluster Nodes of Metal−Organic Frameworks: Structural Diversity and Keys to Reactivity and Catalysis. *Adv. Mater.* **2024**, *36* (5), 2305611.

(2) Xu, W.; Wu, Y.; Gu, W.; Du, D.; Lin, Y.; Zhu, C. Atomic-Level Design of Metalloenzyme-like Active Pockets in Metal-Organic Frameworks for Bioinspired Catalysis. *Chem. Soc. Rev.* **2024**, *53* (1), 137−162.

(3) Mei, D.; Liu, L.; Yan, B. Adsorption of Uranium (VI) by Metal-Organic Frameworks and Covalent-Organic Frameworks from Water. *Coord. Chem. Rev.* **2023**, *475*, 214917.

(4) Siu, B.; Chowdhury, A. R.; Yan, Z.; Humphrey, S. M.; Hutter, T. Selective Adsorption of Volatile Organic Compounds in Metal-Organic Frameworks (MOFs). *Coord. Chem. Rev.* **2023**, *485*, 215119.

(5) Wang, Z.; Chen, J.; Gao, R.; Jiang, L.; Zhang, G.; Zhao, Y.; Miao, Y. B.; Shi, Y. Spatiotemporal manipulation metal−organic frameworks as oral drug delivery systems for precision medicine. *Coord. Chem. Rev.* **2024**, *502* (July 2023), 215615.

(6) Mansi Shrivastav, V.; Dubey, P.; Sundriyal, S.; Tiwari, U. K.; Deep, A. Recent Advances on Core-Shell Metal-Organic Frameworks for Energy Storage Applications: Controlled Assemblies and Design Strategies. *Coord. Chem. Rev.* **2024**, *499* (April 2023), 215497.

(7) Steenhaut, T.; Filinchuk, Y.; Hermans, S. Aluminium-Based MIL-100(Al) and MIL-101(Al) Metal-Organic Frameworks, Derivative Materials and Composites: Synthesis, Structure, Properties and Applications. *J. Mater. Chem. A* **2021**, *9*, 21483−21509.

(8) Evans, H. A.; Mullangi, D.; Deng, Z.; Wang, Y.; Peh, S. B.; Wei, F.; Wang, J.; Brown, C. M.; Zhao, D.; Canepa, P.; Cheetham, A. K. Aluminum Formate Al(HCOO)3: An Earth-Abundant, Scalable, and Highly Selective Material for CO2 Capture. *Sci. Adv.* **2022**, *8* (44), No. eade1473.

(9) Li, P.; Vermeulen, N. A.; Malliakas, C. D.; Gómez-Gualdrón, D. A.; Howarth, A. J.; Mehdi, B. L.; Dohnalkova, A.; Browning, N. D.; O'Keeffe, M.; Farha, O. K. Bottom-up Construction of a Superstructure in a Porous Uranium-Organic Crystal. *Science* **2017**, *356* (6338), 624−627.

(10) Steenhaut, T.; Lacour, S.; Barozzino-Consiglio, G.; Robeyns, K.; Crits, R.; Hermans, S.; Filinchuk, Y. Synthesis, Structure, and Thermal Stability of a Mesoporous Titanium(III) Amine-Containing MOF. *Inorg. Chem.* **2022**, *61* (29), 11084−11094.

(11) Leszczyński, M. K.; Kornowicz, A.; Prochowicz, D.; Justyniak, I.; Noworyta, K.; Lewiński, J. Straightforward Synthesis of Single-Crystalline and Redox-Active Cr(II)-Carboxylate MOFs. *Inorg. Chem.* **2018**, *57* (9), 4803−4806.

(12) Mason, J. A.; Darago, L. E.; Lukens, W. W.; Long, J. R. Synthesis and O2 Reactivity of a Titanium(III) Metal-Organic Framework. *Inorg. Chem.* **2015**, *54* (20), 10096−10104.

(13) Obeso, J. L.; Huxley, M. T.; de Los Reyes, J. A.; Humphrey, S. M.; Ibarra, I. A.; Peralta, R. A. Low-Valent Metals in Metal-Organic Frameworks Via Post-Synthetic Modification. *Angew. Chem., Int. Ed.* **2023**, *62* (49), No. e202309025.

(14) Marzaroli, V.; Spigolon, G.; Lococciolo, G.; Quaretti, M.; Salviati, C.; Kampf, J. W.; Licini, G.; Marchiò, L.; Pecoraro, V. L.; Tegoni, M. Three-Dimensional Porous Architectures Based on Mn II/III Three-Blade Paddle Wheel Metallacryptates. *Cryst. Growth Des.* **2019**, *19* (3), 1954−1964.

(15) Maöczka, M.; Gągor, A.; Hermanowicz, K.; Sieradzki, A.; MacAlik, L.; Pikul, A. Structural Magnetic and Phonon Properties of Cr(III)-Doped Perovskite Metal Formate Framework [(CH3)-2NH2][Mn(HCOO)3]. *J. Solid State Chem.* **2016**, *237*, 150−158.

https://doi.org/10.1021/acs.inorgchem.4c05337
Inorg. Chem. XXXX, XXX, XXX−XXX

(16) Yu, S.; Yu, H.; Si, P.; Wang, Z.; Wang, B.; Lin, W. Preparation of Nanoscale Cationic Metal-Organic Framework Nano Mn(Iii)-TP for Theranostics Based on Valence Changes. *J. Mater. Chem. B* **2022**, *10* (43), 8988−8995.
(17) Reinsch, H.; Stock, N. Formation and Characterisation of Mn-MIL-100. *CrystEngcomm* **2013**, *15* (3), 544−550.
(18) Xiao, Y.; Li, M.; Chen, J. R.; Lian, X.; Huang, Y. L.; Huang, X. C. The Missing MIL-101(Mn): Geometrically Guided Synthesis and Topologically Correlated Valence States. *Inorg. Chem. Front.* **2022**, *348*, 6124−6132.
(19) Yu, K.; Zhang, G.; Chai, H.; Qu, L.; Shan, D.; Zhang, X. Two-Stage Ligand Exchange in Mn(III)-Based Porphyrinic Metal−organic Frameworks for Fluorescence Water Sensing. *Sens. Actuators, B* **2022**, *362* (March), 131808.
(20) Yu, K.; Puthiaraj, P.; Ahn, W. S. One-Pot Catalytic Transformation of Olefins into Cyclic Carbonates over an Imidazolium Bromide-Functionalized Mn(III)-Porphyrin Metal−Organic Framework. *Appl. Catal., B* **2020**, *273* (April), 119059.
(21) Song, G.; Shi, G.; Chen, L.; Wang, X.; Sun, J.; Yu, L.; Xie, X. Different Degradation Mechanisms of Low-Concentration Ozone for MIL-100(Fe) and MIL-100(Mn) over Wide Humidity Fluctuation. *Chemosphere* **2022**, *308* (P2), 136352.
(22) Chen, D.; Zhang, Y.; Mao, P.; Jiang, X.; Li, J.; Sun, A.; Shen, J. Carbon Black Supported on a Mn-MIL-100 Framework as High-Efficiency Electrocatalysts for Nitrophenol Reduction. *J. Electroanal. Chem.* **2021**, *903* (May), 115824.
(23) Ha, Y.; Mu, M.; Liu, Q.; Ji, N.; Song, C.; Ma, D. Mn-MIL-100 Heterogeneous Catalyst for the Selective Oxidative Cleavage of Alkenes to Aldehydes. *Catal. Commun.* **2018**, *103* (135), 51−55.
(24) Huang, H.; Chen, C.; Yang, R.; Yu, Y.; Albilali, R.; He, C. Remarkable Promotion Effect of Lauric Acid on Mn-MIL-100 for Non-Thermal Plasma-Catalytic Decomposition of Toluene. *Appl. Surf. Sci.* **2020**, *503* (July2019), 144290.
(25) Zhang, W.; Shi, Y.; Li, C.; Zhao, Q.; Li, X. Synthesis of Bimetallic MOFs MIL-100 (Fe-Mn) as an Efficient Catalyst for Selective Catalytic Reduction of NO x with NH 3. *Catal. Lett.* **2016**, *146* (10), 1956−1964.
(26) Dyadkin, V.; Pattison, P.; Dmitriev, V.; Chernyshov, D. A New Multipurpose Diffractometer PILATUS@SNBL. *J. Synchrotron Radiat.* **2016**, *23* (3), 825−829.
(27) Favre-Nicolin, V.; Černý, R. FOX Free Objects for Crystallography": A Modular Approach to Ab Initio Structure Determination from Powder Diffraction. *J. Appl. Crystallogr.* **2002**, *35*, 734−743.
(28) Roisnel, T.; Rodríguez-Carvajal, J. WinPLOTR: A Windows Tool for Powder Diffraction Pattern Analysis. *Mater. Sci. Forum.* **2001**, *378* (I), 118−123.
(29) Agilent *CrysAlisPro, V 1.171. 37.35*; Agilent Technlogies, 2014.
(30) Sheldrick, G. M. SHELXT - Integrated Space-Group and Crystal-Structure Determination. *Acta Crystallogr., Sect. A: Found. Crystallogr.* **2015**, *71* (1), 3−8.
(31) Sheldrick, G. M. Crystal Structure Refinement with SHELXL. *Acta Crystallogr., Sect. C: Struct. Chem.* **2015**, *71* (Md), 3−8.
(32) Spek, A. L. PLATON SQUEEZE: A Tool for the Calculation of the Disordered Solvent Contribution to the Calculated Structure Factors. *Acta Crystallogr., Sect. C: Struct. Chem.* **2015**, *71*, 9−18.
(33) Fitch, A.; Dejoie, C.; Covacci, E.; Confalonieri, G.; Grendal, O.; Claustre, L.; Guillou, P.; Kieffer, J.; De Nolf, W.; Petitdemange, S.; Ruat, M.; Watier, Y. ID22 - the High-Resolution Powder-Diffraction Beamline at ESRF. *J. Synchrotron Radiat.* **2023**, *30*, 1003−1012.
(34) Chupas, P. J.; Qiu, X.; Hanson, J. C.; Lee, P. L.; Grey, C. P.; Billinge, S. J. L. Rapid-Acquisition Pair Distribution Function (RA-PDF) Analysis. *J. Appl. Crystallogr.* **2003**, *36* (6), 1342−1347.
(35) Yang, X.; Juhas, P.; Farrow, C. L.; Billinge, S. J. L.XPDFsuite: An End-to-End Software Solution for High Throughput Pair Distribution Function Transformation, Visualization and Analysis, *arXiv*, **2014**.
(36) Johansen, F. L.; Anker, A. S.; Friis-Jensen, U.; Dam, E. B.; Jensen, K. M. Ø.; Selvan, R. A GPU-Accelerated Open-Source Python Package for Calculating Powder Diffraction, Small-Angle-, and Total Scattering with the Debye Scattering Equation. *J. Open Source Softw.* **2024**, *9* (94), 6024.
(37) Momma, K.; Izumi, F. VESTA: A Three-Dimensional Visualization System for Electronic and Structural Analysis. *J. Appl. Crystallogr.* **2008**, *41* (3), 653−658.
(38) Hong, D. Y.; Hwang, Y. K.; Serre, C.; Férey, G.; Chang, J. S. Porous Chromium Terephthalate MIL-101 with Coordinatively Unsaturated Sites: Surface Functionalization, Encapsulation, Sorption and Catalysis. *Adv. Funct. Mater.* **2009**, *19* (10), 1537−1552.
(39) Serre, C.; Mellot-Draznieks, C.; Surblé, S.; Audebrand, N.; Filinchuk, Y.; Férey, G. Role of Solvent-Host Interactions That Lead to Very Large Swelling of Hybrid Frameworks. *Science* **2007**, *315* (5820), 1828−1831.
(40) Millange, F.; Walton, R. I. MIL-53 and Its Isoreticular Analogues: A Review of the Chemistry and Structure of a Prototypical Flexible Metal-Organic Framework. *Isr. J. Chem.* **2018**, *58* (9), 1019−1035.
(41) Thom, A. J. R.; Turner, G. F.; Davis, Z. H.; Ward, M. R.; Pakamorė, I.; Hobday, C. L.; Allan, D. R.; Warren, M. R.; Leung, W. L. W.; Oswald, I. D. H.; Morris, R. E.; Moggach, S. A.; Ashbrook, S. E.; Forgan, R. S. Pressure-Induced Postsynthetic Cluster Anion Substitution in a MIL-53 Topology Scandium Metal-Organic Framework. *Chem. Sci.* **2023**, *14* (28), 7716−7724.
(42) Morelli Venturi, D.; Guiotto, V.; D'Amato, R.; Calucci, L.; Signorile, M.; Taddei, M.; Crocellà, V.; Costantino, F. Solvent-Free Synthesis of a New Perfluorinated MIL-53(Al) with a Temperature-Induced Breathing Effect. *Mol. Syst. Des. Eng.* **2023**, *8* (5), 586−590.
(43) Loiseau, T.; Mellot-Draznieks, C.; Muguerra, H.; Férey, G.; Haouas, M.; Taulelle, F. Hydrothermal Synthesis and Crystal Structure of a New Three-Dimensional Aluminum-Organic Framework MIL-69 with 2,6-Naphthalenedicarboxylate (Ndc), Al(OH)(Ndc)·H2O. *C. R. Chim.* **2005**, *8* (3−4), 765−772.
(44) Wang, X.; Samarasekere, P.; Jacobson, A. J. Synthesis and Single Crystal Structures of V(OH)Ndc·H2O, V(OH)Ndc, and VOndc. *Microporous Mesoporous Mater.* **2018**, *267* (March), 20−23.
(45) Rabe, T.; Pewe, H.; Reinsch, H.; Willhammar, T.; Svensson Grape, E.; Stock, N. Influence of the Substitution Pattern of Four Naphthalenedicarboxylic Acids on the Structures and Properties of Group 13 Metal-Organic Frameworks and Coordination Polymers. *Dalt. Trans.* **2020**, *49* (15), 4861−4868.
(46) López-García, C.; Canossa, S.; Hadermann, J.; Gorni, G.; Oropeza, F. E.; De La Peña O'Shea, V. A.; Iglesias, M.; Angeles Monge, M.; Gutiérrez-Puebla, E.; Gándara, F. Heterometallic Molecular Complexes Act as Messenger Building Units to Encode Desired Metal-Atom Combinations to Multivariate Metal-Organic Frameworks. *J. Am. Chem. Soc.* **2022**, *144* (36), 16262−16266.
(47) Choi, S. B.; Seo, M. J.; Cho, M.; Kim, Y.; Jin, M. K.; Jung, D. Y.; Choi, J. S.; Ahn, W. S.; Rowsell, J. L. C.; Kim, J. A Porous and Interpenetrated Metal-Organic Framework Comprising Tetranuclear Iron III-Oxo Clusters and Tripodal Organic Carboxylates and Its Implications for (3,8)-Coordinated Networks. *Cryst. Growth Des.* **2007**, *7* (11), 2290−2293.
(48) Dong, X. Y.; Wang, R.; Li, J. B.; Zang, S. Q.; Hou, H. W.; Mak, T. C. W. A tetranuclear Cu4(μ3-OH)2-based metal−organic framework (MOF) with sulfonate−carboxylate ligands for proton conduction. *Chem. Commun.* **2013**, *49* (90), 10590−10592.
(49) Wemple, M. W.; Coggin, D. K.; Vincent, J. B.; McCusker, J. K.; Streib, W. E.; Huffman, J. C.; Hendrickson, D. N.; Christou, G. New Tetranuclear Metal Carboxylate Clusters with the [M4(. *J. Chem. Soc. Dalt. Trans.* **1998**, *4* (21), 719−726.
(50) Christiansen, T. L.; Cooper, S. R.; Jensen, K. M. O. There's No Place like Real-Space: Elucidating Size-Dependent Atomic Structure of Nanomaterials Using Pair Distribution Function Analysis. *Nanoscale Adv.* **2020**, *2* (6), 2234−2254.
(51) Castillo-Blas, C.; Moreno, J. M.; Romero-Muñiz, I.; Platero-Prats, A. E. Applications of Pair Distribution Function Analyses to the Emerging Field of: Non-Ideal Metal-Organic Framework Materials. *Nanoscale* **2020**, *12* (29), 15577−15587.

https://doi.org/10.1021/acs.inorgchem.4c05337
Inorg. Chem. XXXX, XXX, XXX−XXX

(52) Terban, M. W.; Billinge, S. J. L. Structural Analysis of Molecular Materials Using the Pair Distribution Function. *Chem. Rev.* **2022**, *122* (1), 1208−1272.
(53) Pallach, R.; Keupp, J.; Terlinden, K.; Frentzel-Beyme, L.; Kloß, M.; Machalica, A.; Kotschy, J.; Vasa, S. K.; Chater, P. A.; Sternemann, C.; Wharmby, M. T.; Linser, R.; Schmid, R.; Henke, S. Frustrated Flexibility in Metal-Organic Frameworks. *Nat. Commun.* **2021**, *12* (1), 4097.
(54) Pallach, R.; Weiß, J. B.; Vollmari, K.; Henke, S. Entropy Driven Disorder-Order Transition of a Metal-Organic Framework with Frustrated Flexibility. *APL Mater.* **2023**, *11* (4), 1041118.

https://doi.org/10.1021/acs.inorgchem.4c05337
Inorg. Chem. XXXX, XXX, XXX−XXX